The Heat Balance in the Western Equatorial Pacific Warm Pool during the Westerly Wind Bursts: A Case Study①②

Liu Hailong (刘海龙), Zhang Xuehong (张学洪), and Li Wei (李 薇)

LASG, Institute of Atmospheric Physics, Beijing 100029

(Received September 1, 2000)

ABSTRACT

The responses of sea surface temperature (SST) in the western equatorial Pacific warm pool to the westerly wind bursts (WWBs) play an important role in the relationship between WWB and ENSO. By using data collected from eight buoys of TOGA (Tropical Ocean–Global Atmosphere)—COARE (Coupled Ocean–Atmosphere Response Experiment), the heat balances of the upper ocean in the western equatorial Pacific around 0°, 156°E during two WWB events were calculated according to Stevenson and Niiler's (1983) method. In both events, SST increased before and after the WWBs, while decreased within the WWBs. The SST amplitudes approximated to 1°C. Although sometimes the horizontal heat advections may become the biggest term in the heat balance, the variation of SST was dominated by the surface heat flux. On the other aspect, some different features of the two events are also revealed. The two cases have different variation of mixed layer depth. The depth of mixed layer is almost double in the first case (35 m to 70 m), which is caused by Ekman convergence, while only 10m increments due to entrainment in the second one. There are also differences in the currents structure. The different variations of thermal and currents structure in the mixing layers accounted for the different variation of the heat balance during the two events, especially the advection and residue terms. The seasonal variation of SST in this area is also investigated simply. The first WWB event happened just during the seasonal transition. So we considered that it is a normal season transition rather than a so–called anomaly. That also suggested that the seasonal distinction of the WWB is worthy of more attention in the researches of its relationship to ENSO.

Key words: Westerly wind burst, The western equatorial Pacific warm pool, Heat balance

1. Introduction

The climatological wind speed is relatively small over the surface of the western Pacific warm pool with the mean magnitude of 1 m s^{-1} (Sadler et al., 1987). There are, however, the so–called 'Westerly Wind Burst' (WWB) events during the period from November to next April (Luther, et al., 1983). A typical WWB has the duration of several days with an averaged wind speed of 10 m s^{-1}. The coherent structure spans over 10°–30° in longitude and 3°–5° in latitude (Harrison and Giese, 1991). WWBs have very vigorous dynamics of their own on

①This work was co–supported by the National Key Project (Grant No. 96–908–02–03), the National Natural Science Foundation of China (Grant No. 4982–3002) and Chinese Academy of Sciences under Grant "Hundred Talents" for "Validation of Coupled Climate models"

②The Chinese version of this paper has been accepted by *Chinese Journal of Atmospheric Sciences.*

intraseasonal timescale (Godfrey et al., 1998). Furthermore, the occurrences of WWB are usually associated with the active phase of Intraseasonal Oscillation (ISO) in atmosphere (Kiladis et al., 1994). In recent researches, the interannual variability of WWB has been suggested to play an important role in triggering El Niño–Southern Oscillation (ENSO) events. It has been found in the observational studies that WWB tends to be more prevalent over the central–western equatorial Pacific before an ENSO event (Luther et al., 1983), which is also the years with strong ISO activities (Nakazawa, 1988).

In the earlier studies, more attention has been paid to the influence of WWB on the sea surface temperature (SST) anomaly in the eastern equatorial Pacific on interannual timescale, while the interaction between WWB and SST anomalies in the warm pool on the intraseasonal time scale has not been well documented. The accomplishment of TOGA (Tropical Ocean–Global Atmosphere) COARE (Coupled Ocean–Atmosphere Response Experiment) makes it possible to investigate the SST variation during the process of WWBs in the warm pool. The response of heat balance of the upper ocean in the warm pool to WWBs were systematically analyzed by Cronin and McPhaden (1997, hereafter CM) for the first time, which suggests that SST increase due to gaining heat from surface flux both prior and posterior to the WWB whilst SST decrease due to losing heat from surface within the WWB. The role of advection is complicated for it is dependent on the varieties in both directions of current and of temperature gradient. Based on the data from drift buoy in TOGA–COARE, Ralph et al. (1997) found that SST decreased during the WWB in December 1992 in the warm pool within which SST is warmer in the east than in the west. Feng et al. (1998) calculated the separate budget of heat and salinity within upper ocean in the warm pool during TOGA–COARE and pointed out that the contribution of advection is not negligible in either balance.

In short, it comes to an agreement in two points with respect to the response of heat balance in the warm pool to the WWB on intraseasonal time scale in the current studies. First and foremost, it is the surface heat flux that controls the SST variation in the warm pool. Secondly, the advection has much complexity and sometimes makes a dominant factor in the heat balance. It should be noted that due to insufficient long duration and high frequency observational data, especially subsurface data, the current researches are based on case study of WWB. So our knowledge about ocean response to WWB is also some segments. The comparison of heat balance in upper ocean between different WWB cases is necessary to obtain a further understanding to the influence of WWBs on SST in the warm pool and, furthermore, to ENSO event.

The buoy data in TOGA–COARE are used to calculate the heat balance of the upper ocean in the western Pacific warm pool around the Intensive Observation Period (IOP) in the present study. Two WWBs are covered and their effects on SST variation are compared with regards to the energy budget. The buoy data are described in the next section. In Section 3, the details of the method used to calculate the heat balance, as well as the error analysis, are given. The results and discussion are presented in Section 4. The main conclusions are summarized in Section 5.

2. Buoy data

Two overlapped time series of buoy data from TOGA–COARE are analyzed. The first segment has the length of 90 days, spanning from 19 September to 17 December 1992. The second one is from 22 October 1992 to 15 January 1993 covering 86 days in total. There are 8

buoys from different sources in the investigated region (2°S–2°N, 154°–158°E) (see Table 1), some of which belong to the array of TOGA–TAO (Tropical Atmosphere and Ocean) observation and the other are supplemented during the IOP, such as the IMET (Improved Meteorology) buoy and ADCP (Acoustic Doppler Current Profiler) measurement buoy from University of South Florida (USF).

Table 1. The location, source and their symbol in this study of 8 buoys

Symbol	A	B	C	D	E	F	G	H
Location	(0°,156°E)	(1.75°S,156°E)	(0°,154°E)	(2°N,156°E)	(2°S,156°E)	(0°,158°E)	(75°N,156°E)	(75°S,156°E)
Source	TAO	IMET	TAO	TAO	TAO	TAO	USF	USF

2.1 *Time series* 1 (TS1, *see Table* 2)

Data used in TS1 are mainly from buoy A. Sea temperature is measured at 10 layers, located at 1 m (surface), 5 m, 11 m, 20 m, 33 m, 57 m, 79 m, 83 m, 107 m, and 132 m, respectively. The salinity is observed at 1 m (surface), 5 m, 11 m, 33 m, 57 m, 83 m, and 132 m. ADCP provides current data at intervals of five meters spanning from 10 m to 255 m in depth. Daily sea temperature data, measured at depths of 1 m, 25 m, 50 m, 75 m, 100 m, 125 m, 150 m, and 200 m, from 4 TAO buoys (C, D, E, F) around buoy A are also used to calculate the advection.

Table 2. Buoys and their measurement in time series 1

Buoy	Surface							Sub–surface		
	Wind vector	Air temperature	Relative humidity	Short wave radiation	precipitation	Sea temperature	salinity	Sea temperature	salinity	current
A	hourly	hourly	hourly	hourly	hourly	daily	hourly	hourly	hourly	hourly
C						daily		daily		
D						daily		daily		
E						daily		daily		
F						daily		daily		

2.2 *Time series* 2 (TS2, *see Table* 3)

Surface and sub–surface data are obtained mainly from buoys B and F. As in TS1, temperatures from buoys C, D, E, F are used in calculating the advection. The current, however, is from the ADCP in buoys G and H. The error induced by the replacement of current measurement will be discussed in the next section.

3. Method and error estimate

The diagnosis of the heat balance is based on the method of Stevenson and Niiler (1983). Details on the parameterization are referred to CM. Vertically averaged, the heat balance of the upper ocean takes the form

$$\rho C_p h\frac{\partial T_a}{\partial t} = (Q_0 - Q_{pen}) - \rho C_p h(\vec{V}_a \cdot \nabla T_a) - (\rho C_p \nabla \cdot \int_{-h}^{0} T'\vec{V}'dz)$$
$$-\left[\rho C_p (T_a - T_{-h})\left(\frac{dh}{dt} + w_{-h}\right)\right] + Q_{-h}, \quad (1)$$

where ρ is the density of sea water, C_p is the specific heat at constant pressure, $\rho C_p = 4.008 \times 10^6$ J °C^{-1}m^{-3}, h is the depth of mixed layer, defined as the distance from surface to a specified potential density (σ_θ) surface ($\sigma_\theta = 21.8$ kgm^{-3}). h is also determined by the level of isothermal surface of 28.5°C when the potential density is unable to be fixed. It has been testified that the error due to the replacement of depth is negligible (not shown). Q_0 is the net downward heat flux; Q_{pen} is the shortwave radiation penetrating through the mixed layer.

The mixed layer depth also has other definitions. The critical gradient of density is often employed. For example, the mixed layer depth can be defined as the first depth below the surface at which the vertical temperature gradient exceeds 5°C / 100 m. Comparing with these three definitions (Fig. 1), we found that the lines of 21.8 kgm^{-3} and 28.5°C are almost overlapping during the majority period of time, and the first line of 5°C / 100 m below the surface is just above the other two lines. The specified potential density or temperature just resides on a strong vertical gradient of temperature. So the definition in our article is fairly reasonable.

Table 3. Buoys and their measurement in time series 2

Buoy	Surface									Sub-surface		
	Wind vector	Air temperature	pressure	Relative humidity	Short wave radiation	Long wave radiation	precipitation	Sea temperature	salinity	Sea temperature	salinity	current
B	hourly	hourly	hourly	hourly	hourly	hourly	hourly	hourly	hourly			
C										daily		
D								daily		daily		
E								daily		daily		
F								daily		daily		
G												daily
H												daily

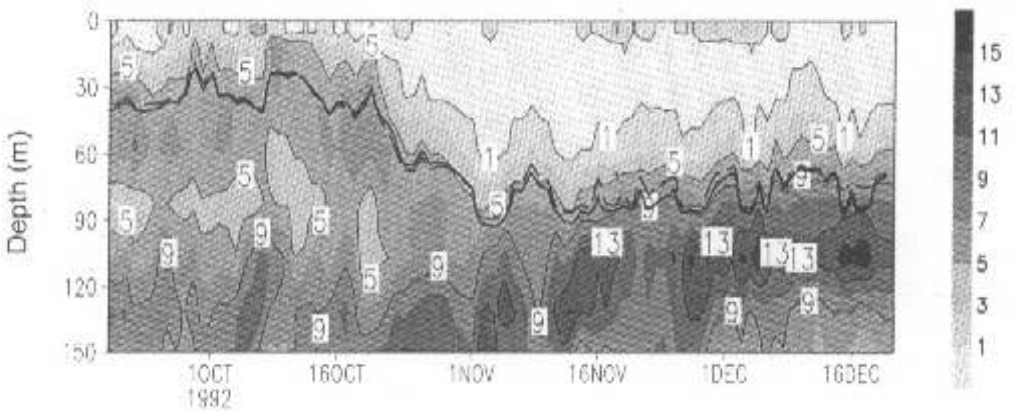

Fig. 1. The vertical temperature gradient (shaded, unit is °C / 100 m, CI = 2), the potential density at 21.8 kgm^{-3} (solid line) and the sea temperature at 28.5°C (dashed line).

Subscript 'a' denotes the vertical average within the mixed layer, which is expressed as

$$( )_a = \frac{1}{h}\int_{-h}^{0}( )dz.$$

T_a and $\vec{V}_a$ are the temperature and current vector averaged within the mixed layer, respectively. T_{-h} and w_{-h} are the temperature and vertical velocity at the bottom of the mixed layer. T' (or $\vec{V}'$) is the departure between T (or $\vec{V}$) and T_a (or $\vec{V}_a$). That is

$$T' = T - T_a, \quad \vec{V}' = \vec{V} - \vec{V}_a.$$

Q_{-h} is the turbulent dissipation of heat at the bottom of mixed layer.

It has been noted by Stevenson and Niiler (1983) and CM that T_a reflects the oscillation of SST in low frequency (with period longer than synoptic scale), implying that T_a is suitable to represent the response of SST to the WWB.

The calculating of each terms in (1) are as follows.

(1) $\rho C_p h\frac{\partial T_a}{\partial t}$ represents the heat storage within the mixed layer, where T_a is obtained based on observation from buoys *A* and *E* for TS1 and TS2, respectively.

(2) Q_0 consists of four components, solar radiation, long wave radiation, latent heat flux and sensible heat flux. These terms are got from data observed by buoys *A* and *B* in TS1 and TS2, respectively. The solar radiation is from observation. The long wave radiation is derived from an experimental formula (Fung et al., 1984) in TS1 and is directly measured in TS2. Latent and sensible heat fluxes are derived from the TOGA–COARE bulk formulae (version 2.5b) (Fairall et al., 1996).

(3) Q_{pen} is parameterized according to the method of Siegel et al. (1995).

(4) $-\rho C_p h(\vec{V}_a \cdot \nabla T_a)$ is the temperature advection averaged over the mixed layer. For TS1, vertically averaged current speed from buoy A and sea temperature from buoys C, D, E and F are utilized. For TS2, current is taken as the mean of buoys G Sand H and h is from buoy E.

(5) The last three terms make up the residue.

The data error in TS1 has been estimated by CM. Separate error during the 55 days superposed in two time series (from 22 October to 17 December 1992) is compared to examine the error of data in TS2. Overall, the variation of each component in (1) is consistent in two time series, except for the term of residue (Fig. 2). It can also be seen from the correlation listed in Table 4. The root–mean–square error is either comparable with or smaller than the corresponding standard deviation of the low–pass–filtered (5 days) data in terms of net surface heat flux, heat storage, advection and Q_{pen}, while it is not the case for residue (Table 4).

Table 4. Comparison of data between two time series

Heat flux	Time mean ($W m^{-2}$)		Standard deviation to low–pass–filtered data (5 days) ($W m^{-2}$)		Correlation of low–pass–filtered data from 55 superposed days	Root–mean–square of low–pass–filtered data from 55 superposed days ($W m^{-2}$)
	TS1	TS2	TS1	TS2		
Net surface heat flux	−0.5	13.2	78.9	61.3	0.95	37.4
Heat storage	−0.4	−21.8	137	127.6	0.71	111.5
Q_{pen}	−7.5	−0.7	8	0.2	0.91	0.28
Advection	24.1	0.8	62.7	32.1	0.99	19.1
Residue	−16.7	−35.1	83	88.9	0.25	139.7

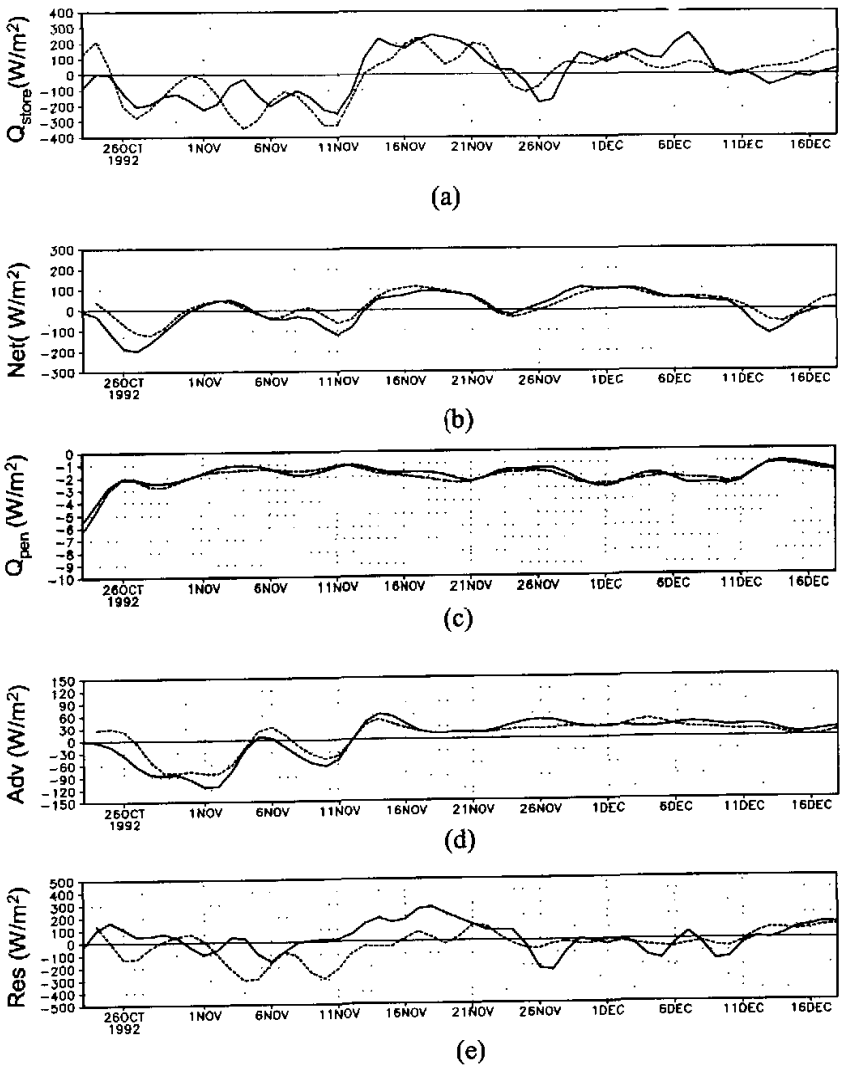

Fig. 2. Five-day low-pass filtered terms of the heat balance during overlapped part of TS1 (solid) and TS2 (dashed) (from 22 Oct. 1992 to 17 Dec. 1992). (a) heat storage, (b) surface heat flux, (c) penetrated shortwave radiation, (d) advection, (e) residue.

4. Results

4.1 *The large-scale climatic background during TOGA-COARE IOP*

Before TOGA-COARE IOP, which lasted four months (from 1 November 1992 to 28 February 1993), the magnitude and pattern of SST, the mixed layer depth and the trade wind over the western Pacific are all close to the climatology, which suggested that 1991–1992 warm event has already ended. After IOP, however, another warm event appeared in the

equatorial Pacific Ocean (McPhaden, 1993). TOGA–COARE IOP was just operated between the two warm events, so it is significant for ENSO study.

During IOP, three ISO events, named ISO1, ISO2 and ISO3 respectively (Godfrey et al., 1998), happened over the western equatorial Pacific Ocean. They successively formed in the Indian Ocean (about 90°E) and propagated eastward at different speeds. The three events arrived at 150°–160°E in mid–October, mid–December and late January respectively and disappeared around the Date Line on the way (Godfrey et al., 1998). When ISOs got the western equatorial Pacific, zonal winds turned to the west, we called these three processes WWB1, WWB2 and WWB3 (Godfrey et al., 1998). In this paper, only WWB1 and WWB2 are included.

4.2 *Comparison of results from WWB1 and WWB2*

According to the well–known periods of the two WWBs, each of both time series is divided into 4 phases. Three of them are investigated in details in the following on the heat budget within the mixed layer. An active phase of either WWB (during WWB) consists of four peaks of enhanced westerly, lasting for 5–7 days for each. The results of WWB1 are compared with that from CM. The comparisons show good agreement although some nonsignificant difference exists. In the following sections, results from WWB1 are not shown and readers can refer to CM. The heat flux is defined as ' positive' if it heats the seawater and vice versa.

4.2.1 *Prior to WWB* (19 *September* –16 *October* 1992 *for WWB1*; 14 *November*–12 *December* 1992 *for WWB2*)

Comparing Fig. 3 with CM's Figs. 3a, 4a, 4d and 7, the common feature before both WWB is the weak zonal wind (mean value of 4.2 m / s for WWB1 and 2.9 m / s for WWB2). In addition, daily mean of SST increases and the difference between T_a and SST is relatively prominent in this period. The major distinction between WWB1 and WWB2 is the opposite direction of zonal current at surface. The depth of mixed layer also has remarkable discrepancy between WWB1 (35 m) and WWB2 (62 m).

The analysis on heat budget (Fig. 4 and CM's Fig. 9) shows that the increase of SST before WWBs is chiefly due to the variation of surface heat flux, of which the shortwave radiation (213.3 W m^{-2} for WWB1 and 214.6 W m^{-2} for WWB2) and latent heat flux (–127.4 W m^{-2} for WWB1 and –85.2 W m^{-2} for WWB2) are the dominant (Table 5). Contribution of advection is of the secondary. On some occasion for WWB1, however, the contribution of strong warm current overrides that of surface heat. The advection keeps weak before WWB2 owing to a weak zonal current. The residue cools SST. The penetrated shortwave radiation is of importance only in the case of shallow mixed layer, such as 35 m before WWB1. It will be neglected in the following discussion.

Table 5. Comparison of the averaged components of net surface heat flux between two time serie

	Net (W m^{-2})		Shortwave (W m^{-2})		Longwave (W m^{-2})		Sensible (W m^{-2})		Latent (W m^{-2})	
	TS1	TS2	TS1	TS2	TS1	TS2	TS1	TS2	TS1	TS2
Prior to WWB	24.8	57.4	213.3	214.6	–49.7	–64.0	–11.4	–7.9	–127.4	–85.2
During WWB	–77.1	–41.0	152.7	149.1	–47.4	–51.3	–17.9	–11.9	–164.6	–126.8
Posterior to WWB	65.1	71.0	212.1	192.0	–45.6	–57.9	–6.4	–7.0	–95.0	–56.1

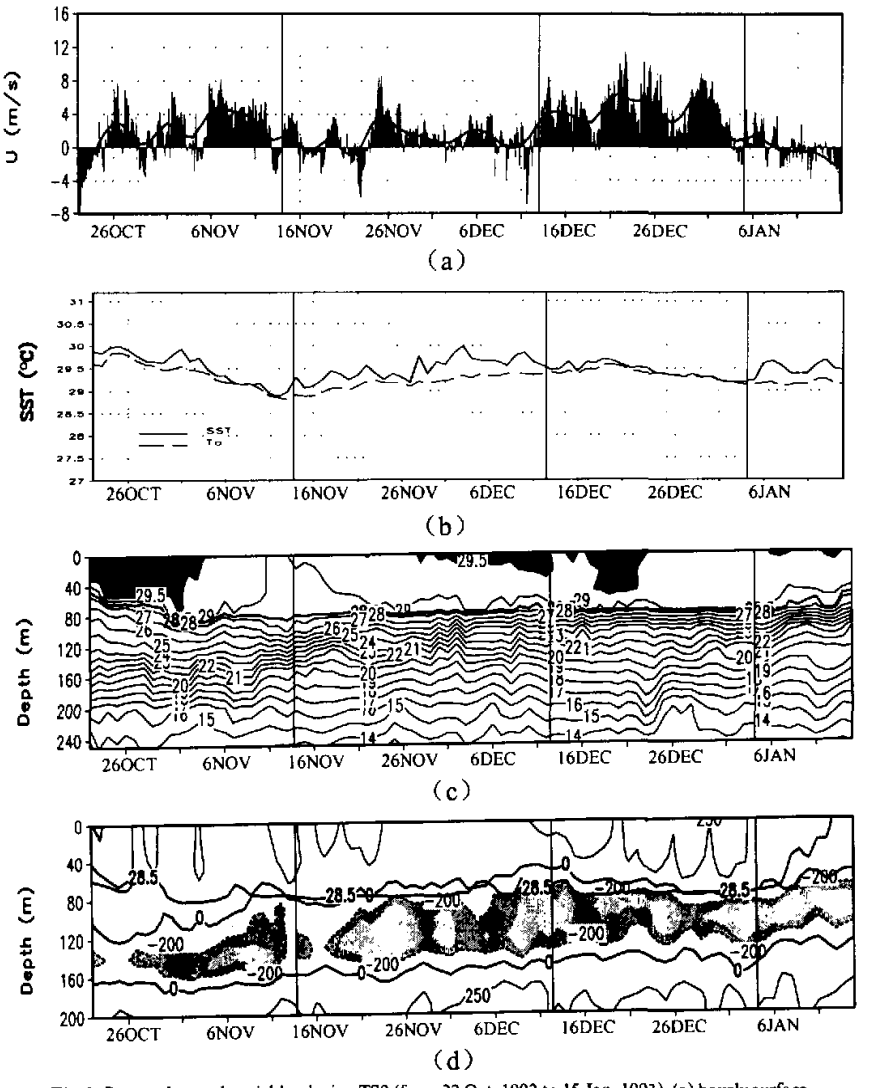

Fig. 3. Buoys observed variables during TS2 (from 22 Oct. 1992 to 15 Jan. 1993), (a) hourly surface zonal wind at buoy B (unit: m s^{-1}), (b) hourly SST (solid) and T_a (dashed) at buoy E (unit: °C), (c) time–depth SST at buoy E (unit: °C),(d) time–depth averaged zonal currents between buoy G and H (unit: mm s^{-1}).

The heat budget is summarized in Figs. 5a and 5d for the time mean of period before WWB1 and WWB2, respectively. The amplitude of SST increase is 1°C before both WWBs. The heat storage before WWB2 (68.5 W m^{-2}) is almost double of that before WWB1 (36.3 W m^{-2}) since the mixed layer in the former is much thicker. Both surface heat and advection flux make SST rise whilst penetrated shortwave radiation and residue cool the mixed layer. The surface heat flux before WWB1 (24.8 W m^{-2}) is less than that before WWB2 (57.4 W m^{-2})

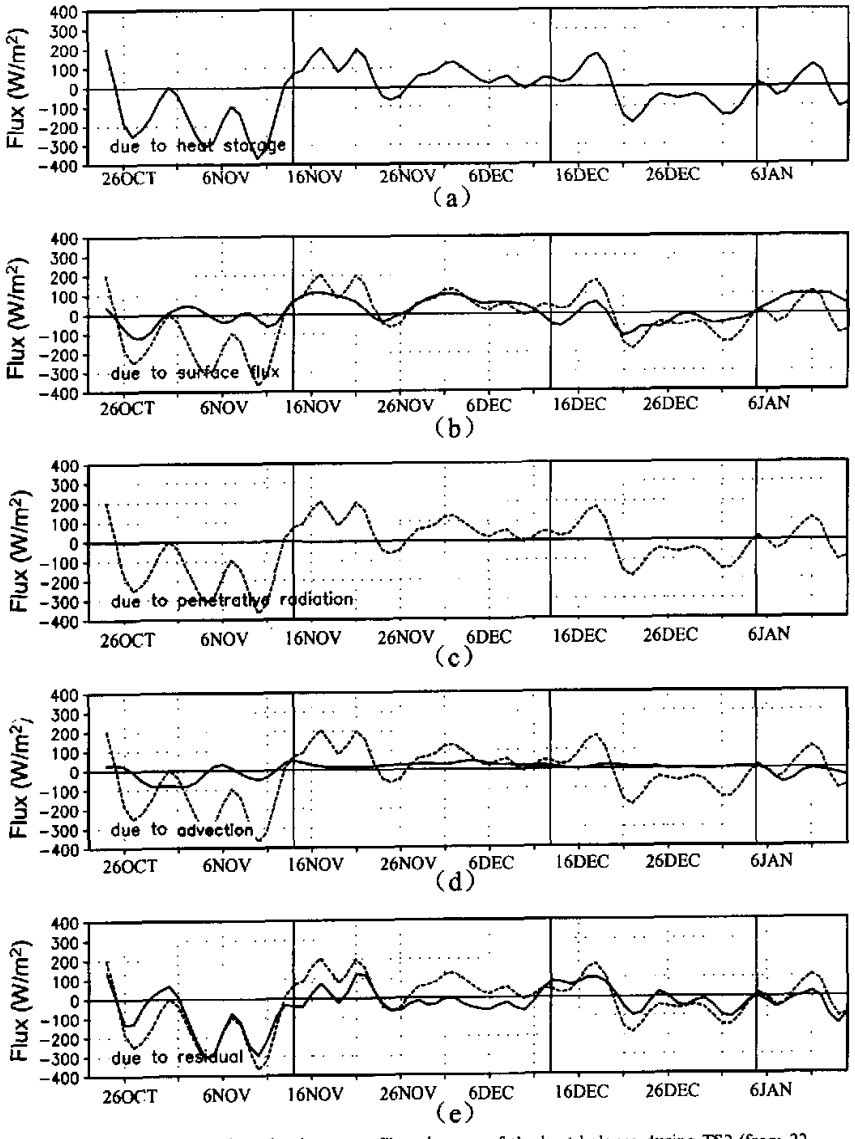

Fig. 4. Solid lines are five-day low-pass filtered terms of the heat balance during TS2 (from 22 Oct. 1992 to 15 Jan. 1993). (a) heat storage, (b) surface heat flux, (c) penetrated shortwave radiation, (d) advection, (e) residue (unit: W m^{-2}); dashed lines in the last four figures are heat storage term.

which may ascribe to the smaller wind speed in the latter case. The differences in advection before WWB1 (60.8 W m^{-2}) and before WWB2 (24.2 W m^{-2}) result from both the stronger surface current and larger temperature gradient. Without consideration of error, the residue is different before two WWBs because of the diversity in the current field and mixed layer.

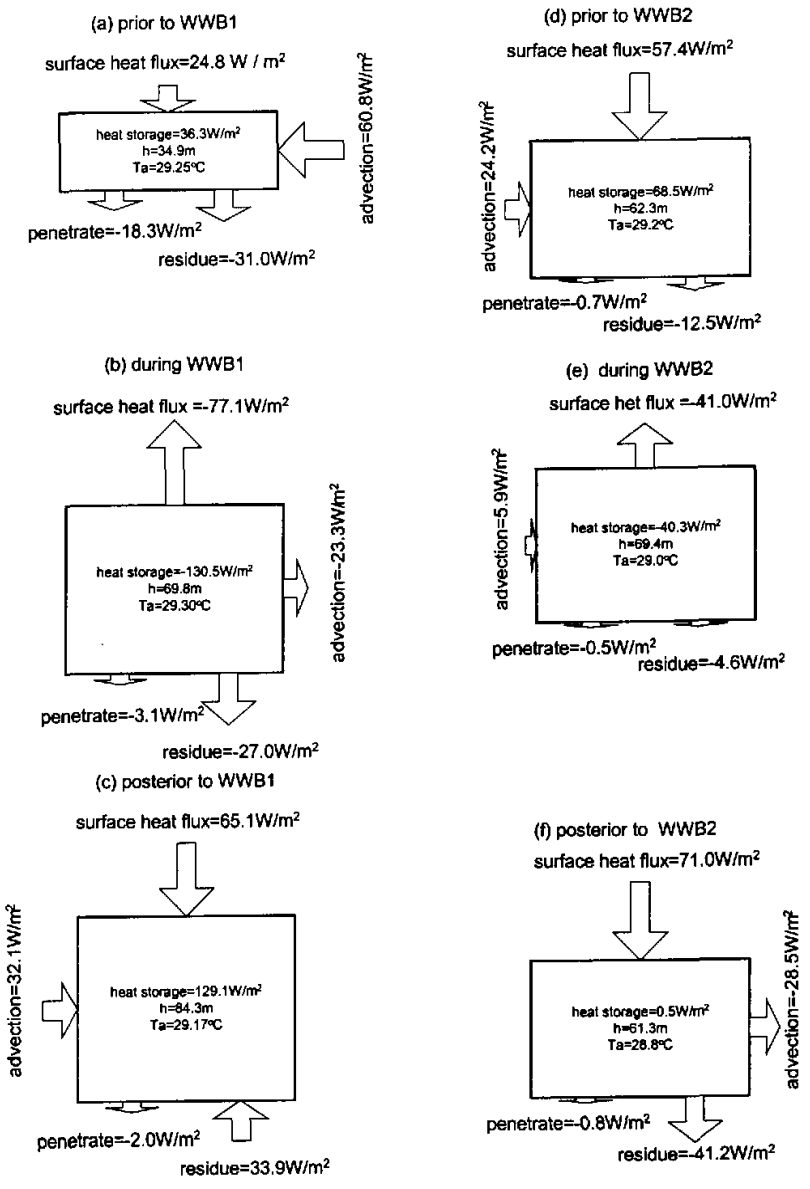

Fig. 5. Period-averaged heat balances of TS1 (a) prior to WWB1, (b) during WWB1 and, (c) posterior to WWB1) and TS2, (d) prior to WWB2, (e) during WWB2 and, (f) posterior to WWB2.

4.2.2 *During WWB* (17 *October*–12 *November* 1992 for *WWB*1; 13 *December* 1992–4 *January* 1993 *for WWB*2)

The westerly wind is strongly intensified during the WWBs and the wind speed averaged for WWB1 and WWB2 reaches 5.7 m / s and 6.1 m / s, respectively (Fig. 3a and CM's Fig.

3a). The amplitude of SST decrease is 1°C for either event (Fig. 3b and CM's Fig. 4a). The SST decrease lags a little the intensified westerly in WWB2 since SST and zonal wind are observed at different buoys that are not exactly at the same position. The depth of mixed layer doubled during WWB1 while varied smaller relative to its original depth during WWB2 (Fig. 3c and CM's Fig. 4d). The westward current become weak and even reversed in mixed layer during WWB1. The eastward current in mixed layer is enhanced during WWB2 (Fig. 3d and CM's Fig. 7). Investigating the current field around 0°, 156°E, we found that there is obvious convergence by the Coriolis force for period 21 October to 24 October (figure omitted). The deepening of mixed layer during WWB1 is mainly the results of the subsidence and wind stir. This is the same as the conclusion drawn by CM. The deepening of mixed layer is remarkable in WWB2, which may be due to the weak wind stir.

The surface heat flux keeps dominant in determining the SST variation during either WWB1 or WWB2 (Fig. 4 and CM's Fig. 9). According to Table 5, there is significant reduction of shortwave radiation and increase of latent heat flux during WWBs, both of which result in the cooling of SST. The contribution of advection is changeful during WWB1. It turns from warm current to cold current due to the variation in both flow direction and temperature gradient. During WWB2, the amount of advection is relatively small for either current speed or temperature gradient is small. The variation of residue is rather complicated. T_a contains more information from ocean when the depth of mixed layer increase, which make for a stronger influence of residue on T_a.

The comparison of amount of each component in heat fluxes averaged during WWBs is shown in Figs. 5b and 5e. The notable difference of heat storage between WWB1 (-130.5 W m^{-2}) and WWB2 (-40.3 W m^{-2}) is explained by the dramatic variation of depth of mixed layer in the former. The role of surface heat flux, penetrated shortwave radiation and residue is to cool T_a. The mean advection is cold current for WWB1 while weak warm current for WWB2.

4.2.3 *Posterior to WWB (13 November–7 December 1992 for WWB1; 5 January–15 January 1993 for WWB2)*

The mean speed of zonal wind reduced to 3.1 m/s and 1.9 m/s after the passage of WWB1 and WWB2 respectively (Fig. 3a and CM's Fig. 3a). The SST was warmed with an amplitude of 1°C after WWB1 and 0.2°C after WWB2 and the discrepancy between T_a and SST was enlarged (Fig. 3b and CM's Fig. 4a). The bottom of mixed layer was raised (Fig. 3c and CM's Fig. 4d) and the zonal current was weak (Fig. 3d and CM's Fig. 7). After WWB2, the eastward surface current was reversed, which was associated with South Equatorial Current. Upwelling brought on by the westward current was one of the important reasons for the lift of mixed layer.

The heat balances after the WWBs are similar to that before the WWBs (Fig. 4 and CM's Fig. 9). The surface heat flux, mainly composed by increase of shortwave radiation and decrease of latent heat, is the dominant term (Table 5). For the fully mixing within the mixed layer, the amount of advection is small for both cases. The role of residue was to heat the seawater after WWB1 while to cool after WWB2. It was argued by CM that the heat comes from the convergence / divergence of shear current in the residue. It also should be noted that the effect of sub–grid process may be important.

For the mean of heat balance (Figs. 5c and 5d), there was also noticeable difference of the heat storage between that after WWB1 (129.1 W m^{-2}) and after WWB2 (0.5 W m^{-2}). The contribution of surface heat flux, which is 65.1 W m^{-2} for WWB1 and 71.0 W m^{-2} for

WWB2, is to increase SST in both cases. The advection has comparable amount in the two cases, only that it is warm current for WWB1 (32.1 W m^{-2}) while cold current for WWB2 (−28.5 W m^{-2}). The sign of residue is also opposite in the two cases.

5. Discussions

There is a common feature in SST variation for both WWBs. SST increases prior to and posterior to the WWB while decreases during the process of WWB with the similar amplitude of 1°C. A cycle of SST variation, consisting of a span of SST increase and a span of SST decrease, has the period of 50–60 days, which is comparable with that of the ISO in atmosphere. WWB has a little impact on the mean SST averaged in two spans. It is consistent with the results from Zhang (1996) that the SST oscillation has a significant period of about 50 days in the western equatorial Pacific on the basis of buoy data from TAO for 3 years.

It should be noted that the characteristics of heat balance in upper ocean are quite distinct from each other in two WWBs. The depth of mixed layer before WWB2 is double that before WWB1, which means a double heat flux is needed to the former to an equivalent amount of temperature variation within the mixed layer. It is one of the major reasons for smaller amplitude of SST variation during WWB2. The heat flux due to advection is much less in WWB2 than in WWB1 since the mean speed of surface current is relatively small in the former. Additionally, stability of the mixed layer, which is determined by both temperature and flow, has a crucial impact on the components of residue. It can be concluded that the thermohaline and current structures play an important role in influencing the surface heat balance besides the effects of the intensity and location of WWB.

In the heat balance, the residue term is the most confusing one. To further understand it, we also estimated the Niiler–Kraus mixing (Niiler and Kraus, 1977) during TS2 comparing with residue term following CM (Fig. 6). The wind stir, free convection and shear instability coefficients are 0.4, 0.6 and 0.6 respectively, which are the same as that of CM. The mixing rate is high during WWB2 and low before and after WWB2. This is different from WWB1

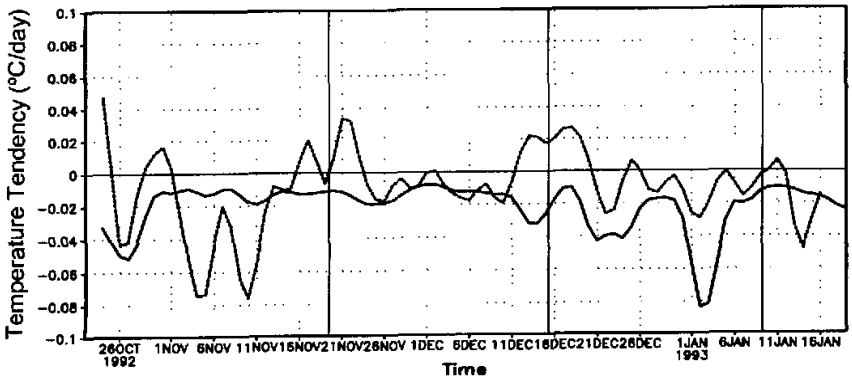

Fig. 6. Niiler–Kraus mixing (solid, m = 0.4, n = 0.6, s = 0.6) and the residue term (dashed) at IMET (1.75°S, 156°E) during TS2 (unit: °C / day).

(CM's Fig. 11b), which has a high mixing rate before WWB and low one in other two periods. So unlike WWB1, in which the deepening of the pycnocline is mainly caused by Ekman convergence, the turbulent mixing due to buoyancy and wind stir is the major factor influencing the deepening of mixing layer depth in WWB2.

WWB1 spanned the seasons from fall to winter. Because of the seasonal transition, there is a different seasonal variation superposed on the intraseasonal variation of upper-ocean owing to WWB. The dramatic deepening of the depth of mixed layer and the reverse of the surface flow direction in WWB1, for example, may be mainly ascribed to seasonal, rather than intraseasonal, variation. It is supported by the tendency of seasonal variation (100-day low-pass filtered) of SST in the warm pool from NCEP reanalysis (Fig. 7). WWB1 appeared when the seasonal variation of SST turned from increase to decrease. The cooling of SST in seasonal variation is notable. In addition, the abnormal structures of thermohaline and current resulting from WWB1 affect the climate background in upper-ocean to the succedent WWB2.

The three WWB events in the winter 1992/1993 have a crucial role in triggering the warm ENSO episode in 1993 (Kessler et al., 1995). It suggests that the intraseasonal air-sea interaction in the tropical western Pacific is of great importance to the coupled system of ENSO on interannual time scale. With regard to the intraseasonal variation, the active ISO over the tropical Indian Ocean and the western Pacific reinforces cloud amount and precipitation. The induced westerly cools SST and meanwhile the cooler SST depresses the deep convection. All the processes compose a negative air-sea feedback. The signal of intraseasonal SST variation propagates eastward and/or affects deeper ocean below the mixed layer. The eastward propagation of sea temperature anomaly in sub-surface can be seen during WWB1 with the speed near that of Kelvin Wave. The intraseasonal oscillation in atmosphere has influences on deeper ocean on a longer term, i.e., interannual, than it has on the upper ocean. The seasonal variation is also related to the WWB-deduced intraseasonal oscillation in upper ocean.

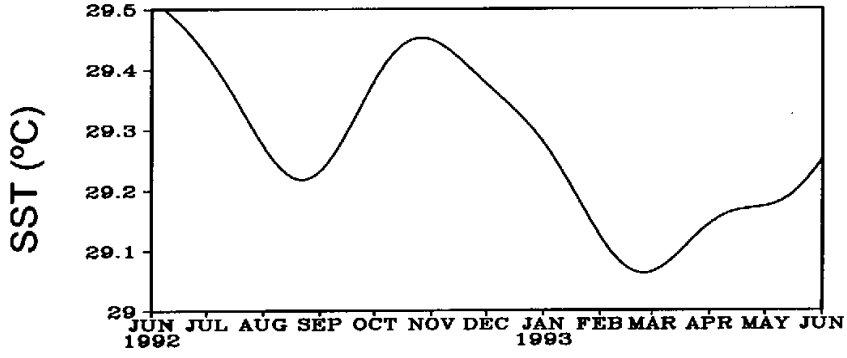

Fig. 7. 100-day low-pass filtered NCEP weekly SST averaged in the western equatorial Pacific warm pool (1.4°S, 154.7°E, 1.4°S, 157.5°E, 1.4°N, 154.7°E and 1.4°N, 157.5°E).

6. Conclusions

The surface heat balance over the western Pacific warm pool is investigated using buoy observations from TOGA–COARE for two WWB cases. The following characteristics of the behavior of surface varieties were found during the process of WWBs:

(1) For both WWB events in TOGA–COARE, there are increases of SST prior to and posterior to the WWB whilst decrease of SST during the WWB with the equivalent amplitude of about 1°C. On the intraseasonal time scale the temperature in the mixed layer is mainly dependent on the surface heat flux. Among the components of heat flux, shortwave radiation and latent heat fluxes are the most important which determine the direction of net heat flux. The role of advection transport is of secondary importance, which overrides the action of surface heat flux in SST variation on some occasions.

(2) There is a remarkable deepening of the mixed layer during the WWB. For WWB1, the depth of mixed layer increases from about 35 m to 70 m due to the Ekman convergence of circulation. For WWB2, the increment of depth of the mixed layer is less than 10 m, which results from the wind stir, circulation structure and the eastward propagation of the WWB.

(3) Comparison of the features of heat balance between the two WWBs show an obvious difference between them. It is ascribed to the different thermohaline structure and circulation field in variant seasonal background. The seasonal distinction of the WWB is worthy of more attention in the researches of its relationship to ENSO.

Precise and accurate observations are still needed to get a proper understanding to the air–sea interaction system over the western Pacific warm pool, which is suggested to play an important role in triggering ENSO event.

The buoy data were obtained from TAO Project Office web site. We are very grateful for Dr. Yu Zuojun to provide the helpful information on TOGA–COARE data set and Dr. Yu Rucong to download the data for us.

REFERENCES

Cronin M. F., and M. J. McPhaden, 1997: The upper ocean heat balance in the western equatorial Pacific warm pool during September–December 1992. *J. Geophys. Res.*, **102**, 8533–8554.

Fairall, C., E. F. Bradley, D. P. Rogers, J. B. Edson, and G. S. Young, 1996: Bulk parameterization of air–sea fluxes for Tropical Ocean–Global Atmosphere Coupled–Ocean Atmosphere Response Experiment algorithm. *J. Geophys. Res.*, **101**, 3747–3764.

Feng, Ming., P. Hacker, and R. Lukas, 1998: Upper ocean heat and salt balances in the response to a westerly wind burst in the western equatorial Pacific during TOGA–COARE. *J. Geophys. Res.*, **103**, 10289–10311.

Fung, I. Y., D. E. Harrison, and A. A. Lacis, 1984: On the variability of the net longwave radiation at the ocean surface. *Rev. Geophys.*, **22**, 177–193.

Godfrey J. S. et al., 1998: Coupled Ocean–Atmosphere Response Experiment (COARE): A interim report. *J. Geophys. Res.*, **103**, 14395–14450.

Harrison, D. E., and B. S. Giese, 1991: Episodes of surface westerly winds as observed from islands in the western tropical Pacific. *J. Geophys. Res.*, **96(suppl.)**, 3221–3237.

Kessler, W. S., M. J. McPhaden, and K. M. Weickmann, 1995: Forcing of intraseasonal Kelvin waves in the equatorial Pacific. *J. Geophys. Res.*, **100**, 10613–10631.

Kiladis, G.N., G.A. Meehl, and K.M. Weickmann, 1994: The large scale circulation associated with westerly wind bursts and deep convection over the western equatorial Pacific. *J. Geophys. Res.*, **99**, 18527–18544.

Luther, D. S., D. E. Harrison, and R. A. Knox, 1983: Zonal winds in the central equatorial Pacific Ocean and El Niño, *Science*, **222**, 327–330.

McPhaden, M. J., 1993: TOGA-TAO and the 1992-93 El Niño-Southern Oscillation event. *Oceanography*, **6**, 36-44.

Nakazawa, T., 1988: Tropical super clusters within intraseasonal variations over the western Pacific. *J. Meteor. Soc. Japan*, **66**, 823-839.

Niiler, P. P., and E. B. Kraus, 1997: One-dimensional models of the upper ocean, in *Modelling and Prediction of the Upper Layers of the Ocean*, edited by E. B. Kraus, Pergamon, Tarrytown, N. Y. 143-172.

Ralph, E. A., K. Bi, P. P. Niiler, and Y. du Penhoat, 1997: a Lagrangian description of the western equatorial Pacific response to the wind burst of December 1992: Heat advection in the warm pool. *J. Climate.*, **10**, 1706-1721.

Sadler, J., M.A. Lander, A.M. Hori and L.K. Oda, 1987: Tropical marine climatic atlas, Volume II, Pacific Ocean, UHME87-02, Department of Meteorology, University of Hawaii, 27 pp.

Sirgel, D. A., J. C. Ohlmann, L. Washburn, R. R. Bidigare, C. T. Nosse, E. Fields and Y. Zhou, 1995: Solar radiation, phytoplankton pigments and the radiant heating of the equatorial Pacific warm pool. *J. Geophys. Res.*, **100**, 4885-4891.

Stevenson, J. W., and P. P. Niiler, 1983: Upper ocean heat budget during the Hawaii-to-Tahiti shuttle experiment. *J. Phys. Oceanogr.*, **13**, 1894-1907.

Zhang Chidong, 1996: Atmospheric intraseasonal variability and mean values of the surface meteorology and air-sea fluxes in the western equatorial Pacific Ocean. *J. Atmos. Sci.*, **53**, 739-758.

西风爆发时赤道西太平洋的热量平衡: 个例分析

刘海龙　张学洪　李　薇

摘　要

赤道西太平洋暖池海表温度 (SST) 对西风爆发(WWB) 的响应是 WWB 与 ENSO 相互作用的一个重要环节。利用 TOGA-COARE 期间暖池海区的 8 个浮标观测资料，根据 Stevenson 和 Niiler(1983)的热量平衡诊断方法，分析了两次 WWB 期间赤道 156°E 附近上层海洋的能量平衡。两次 WWB 期间，SST 都是在 WWB 之前和其后升温，而在 WWB 期间降温，升温和降温的幅度均在 1°C 左右．SST 的变化主要是由海表热通量决定的，部分时段水平热平流也可成为热平衡中的最大项。研究也发现了两次 WWB 期间上层海洋的不同变化特征．第一次 WWB 期间，由于 Ekman 辐合作用，混合层的厚度加深了一倍 (从 34m 到 70m)，而第二次 WWB 期间混合层的厚度仅由于夹卷效应加深了 10m。两次 WWB 期间的流场结构也存在区别。温度场和流场的差异共同解释了两次 WWB 期间上层海洋热平衡的不同变化特征，尤其是平流项和残差项。另外，第一次 WWB 的发生正处于季节转换期，观测 SST 的变化中包含相当程度的季节变化．季节特征也是研究 WWB 与 ENSO 关系时需要考查的一个方面。

关键词: 西风爆发, 赤道西太平洋, 热量平衡